RESEARCH ARTICLE

Unraveling the cause of degradation in Cu(In,Ga)Se$_2$ photovoltaics under potential induced degradation

Zeel Purohit[1,2,3] (iD) | Jorne Carolus[2,3] | Harsh Chaliyawala[4,5] | Shubhendra K. Jain[6] | Abhiram Gundimeda[6,7] | Govind Gupta[6] | Brijesh Tripathi[1] | Michaël Daenen[2,3]

[1] Department of Science, School of Technology, Pandit Deendayal Petroleum University, Gandhinagar, Gujarat, India

[2] Hasselt University, Hasselt, Belgium

[3] Energyville II, Genk, Belgium

[4] Solar Research and Development Center, School of Solar Energy, Pandit Deendayal Petroleum University, Raisan, Gandhinagar, Gujarat, India

[5] Department of Physics, Sardar Vallabhbhai National Institute of technology, Surat, India

[6] Physics of Energy Harvesting, CSIR-National Physical Laboratory, New Delhi, India

[7] Department of Materials Sciences and Metallurgy, University of Cambridge, The Old Schools, Cambridge, UK

Correspondence
Zeel Purohit, Department of Science, School of Technology, Pandit Deendayal Petroleum University, Gujarat, Gandhinagar 382007, India.
Email: zeelpurohit.zp@gmail.com

Abstract

Copper indium gallium diselenide (CIGS) based technology is actively competing in the global photovoltaic market with high conversion efficiency. Commercial CIGS modules are anticipated to perform on rated output in the field condition for 20 years. Potential induced degradation (PID) is considered as one of the critical concerns among all the current reliability assessment issues. PID accelerated tests have been performed on pre-commercial CIGS modules to investigate reduction in electrical performance. We report the severe reduction in electrical performance after PID is correlated to the microstructural and chemical properties of the constituent materials. Under extreme PID stress, the cell surface reveals various defects including crater formation. The aim of this article is to explore the consequences of PID induced craters on the efficiency of CIGS solar cells by investigating material degradation kinetics. In this perspective, we present the root cause of PID in CIGS thin-film modules in relation to microstructural defects by detailed investigation using J-V analysis, field emission scanning electron microscope (FESEM), Raman spectroscopy, X-Ray diffraction (XRD), X-ray photoelectron spectroscopy (XPS) and photoluminescence spectroscopy (PL). This analysis can provide more effective and sustainable research strategies to cultivate more efficient and reliable CIGS technologies in the long run.

KEYWORDS
CIGS, degradation, material analysis, PID

1 | INTRODUCTION

Over the last few decades, chalcopyrite copper indium gallium diselenide (CIGS) based thin film technologies have shown significant developments and penetration in the commercial global market.[1] In addition, a high efficiency of 22.9% has been reported at cell level[2] and at commercial module level it has reached up to 18.72%.[3] Constant efforts have been made by industry and researchers to minimize the cell to module efficiency gap.[4] However, a lot of attention is required to ensure the rated module performance under operating field conditions. Under

extreme environmental impact and high voltage stress conditions, modules undergo mid-life failure which leads to significant loss of efficiency within a short period of time (much lower than rated warranty period). This effect is known as potential induced degradation (PID).[5,6,7] The coercive issues of PID mid-life failures raise a warning alarm for industries to reveal the degradation mechanism to constrain its larger impact on global PV investments. In order to make the CIGS module-based solar industry much more competitive in a sustainable manner, PID analysis is required to be investigated in-depth.

Surprisingly, only few reports have been communicated on PID effect in CIGS solar cells till now. Previous studies demonstrated the effect of glass substrates containing different Na concentrations[8,9] and buffer layers[10] on electrical performance of CIGS thin-film solar cells, to examine PID susceptibility. Sodium (Na) migration and its disturbance in concentration levels are found as the key factor responsible to PID.[8,9,11,12] Light-induced Na migration results in the formation of Na rich spots on zinc oxide aluminum (ZnO:Al) surface and it reacts with atmospheric species like oxygen, carbon and chlorine.[13,14] Furthermore, the ingression of a darkening effect observed in case of tin-oxide and ZnO has been attributed to Na accumulation.[15] There are also reports on the effect of alkali (Na, K) elements on the device performance under damp heat and illumination conditions.[16,17] However, the PID effect associated to material aspects with their chemical kinetics have not been demonstrated yet in detail. Although, there are various reports that suggest a beneficial impact of Na on the performance of CIGS solar cells at lower concentration such as:[18–21] (1) a moderate level of Na concentration (0.1%) improves the grain size of the CIGS, crystal structure quality and orientations (122) by passivation of grain boundaries, (2) it enhances hole concentration and conductivity by creating Na_{Cu} type acceptor defects, (3) it reduces non-radiative centers located at the grain boundaries, (4) it yields the Cu-deficient surface which reduces interfacial recombination found to be beneficial for cell performances. However, a detrimental effect starts when a higher Na concentration beyond 0.1% enters into CdS buffer layer puncturing heterojunction of the device.

While most of earlier studies demonstrated either the impact of alkali elements or stability variation on the CIGS performance, but the root cause of PID in thin-film modules under extreme conditions is yet investigated in-depth.[6,11] Here we report the first study on the identification of craters formation under PID of CIGS solar cell. Moreover, the degradation kinetics have been explained in relation with microstructural defects by detailed investigation using J-V analysis, FESEM, Raman spectroscopy, XRD, X-ray photoelectron spectroscopy (XPS) and PL on commercial CIGS solar cells. Furthermore, the root cause of PID and the consequences of crater formation on electrical performance of the CIGS solar cells have been explored in detail.

2 | EXPERIMENTAL SECTION

2.1 | Fabrications and experimental set-up

Pre-commercial CIGS solar cells have been taken for this study. The cell stack consisted of soda lime glass (SLG)/Molybdenum (Mo)/CIGS absorber layers/cadmium sulphide (CdS) buffer layer/Zinc oxide (ZnO). The Mo layer was deposited on SLG by DC-sputtering, CIGS absorber layers were co-evaporated on Mo-coated soda-lime glass (SLG) following the three-stage process, CdS buffer layer grown by chemical vapor deposition (CVD), ZnO bilayers and contact grids were deposited on to these absorbers. All the samples were exposed to high voltage stress of 1000 V at 85°C in a climate chamber for 70 hours. The positive and negative terminal of the cells were shorted and connected to the negative terminal of the high voltage supply. The positive terminal of the high voltage power supply was connected to a silver foil placed on the device on the glass side.

2.2 | Material characterizations

To explore extreme reduction in J-V performance after PID treatment, the surface morphology was performed on initial and after PID treatment using FESEM, Carl Zeiss, ultra-55, 1–20 kV Oxford Instruments. Furthermore, to investigate the changes in structural phases after PID exposure, XRD measurements were carried out with PAN-alytical's MDP X'Pert-Pro instrument using a 1D PIXcel detector in the Bragg-Brentano configuration with a step size of 0.013° and 400 seconds acquisition time per step. In addition, Micro-Raman analysis was performed using Renishaw inVia system with an excitation laser beam of 532 nm, to detect multi-phase extreme deteriorated regions. The compositional and chemical analysis have been performed using XPS, multi technique surface analysis system (Scienta-Omicron, Germany). Photoluminescence intensity and carrier life time decay measurements (PL) were carried out using an Edinburgh FLS980-d2d2 spectrometer. The excitation arm of the system was equipped with a xenon lamp (450 W). The emission arm was equipped with a standard visible PMT detector.
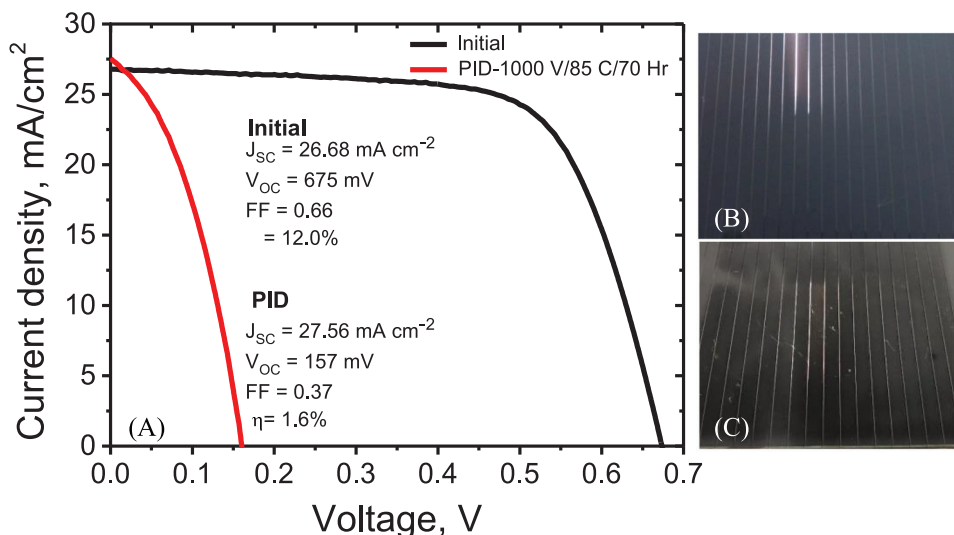
FIGURE 1 (A) J-V characteristics of CIGS solar cells measured under simulated AM 1.5, 100 mW cm^{-2} illuminations for initial and after PID, (B) initial surface of CIGS solar cell and (C) after PID exposure cell surface

TABLE 1 CIGS solar cell performance parameters of initial and after PID treatment

Conditions	J_{sc} [mA]	V_{OC} [V]	R_s [Ω]	R_{sh} [Ω]	FF [%]	η [%]
Initial	26.68	0.67	0.8	10,000	66	12
PID	27.56	0.15	1.5	8.7	37	1.5

Abbreviation: PID, potential induced degradation.

3 | RESULTS AND DISCUSSION

3.1 | Current-voltage (J-V) characteristics of PID affected cells

In order to investigate the effect of high voltage stress of 1000 V at 85°C on CIGS solar cells, J-V performances were measured for the initial case and after PID as shown in Figure 1A. The related photovoltaic performance parameters are shown in Table 1. The PID-treated CIGS solar cell shows a dramatic deterioration in electrical performance as compared to the initial performance. The initial solar cell exhibited J_{SC} of 26.68 mA cm^{-2}, V_{OC} of 0.67 V, FF of 66% and efficiency (η) of 12 %, respectively. The PID treated solar cell demonstrated a drastic reduction in performance as V_{OC} was reduced from 0.67 to 0.15 V, FF decreased from 66% to 37% and η was reduced to 1.6% after 70 hours. The reduction in performance parameters was dominated by a drastic change in series resistance (R_S) and parallel resistance (R_{Sh}) after PID. R_S and R_{Sh} values changed from 0.015 to 0.15 Ω and 10^3 to 150 Ω, respectively. Furthermore, visual inspection demonstrated that the cell's surface color changed from blue to random dark black patches after the

PID treatment. The change in color may shed light on different microstructural features associated to extreme deterioration of efficiency under PID.

3.2 | Microstructural analysis of PID cells

The surface morphology of the CIGS thin-film solar cells for initial samples and PID stressed samples are shown in Figure 2. It can be seen from Figure 2A that an initial cell surface shows a uniform grain distribution. Conversely, Figure 2B shows a non-uniform and defected surface after the PID treatment of 70 hours. In addition, stretch marks have been observed under low magnification at different regions on the PID treated cell's surface, which can be clearly seen in Figure 2C-E. Moreover, the deteriorated surface reveals craters on the PID treated cell surface as shown in Figure 2F-H. The craters pronounced extreme microstructural deformation. Hereafter, EDS analysis has been performed near and within the regions of craters to analyze the presence of associated elements in the deformed regions. A major change in the atomic concentration of O and Zn have been observed on the crater
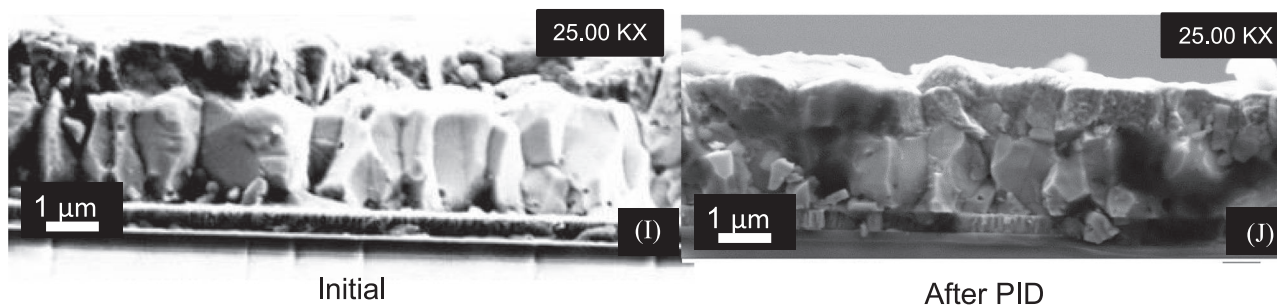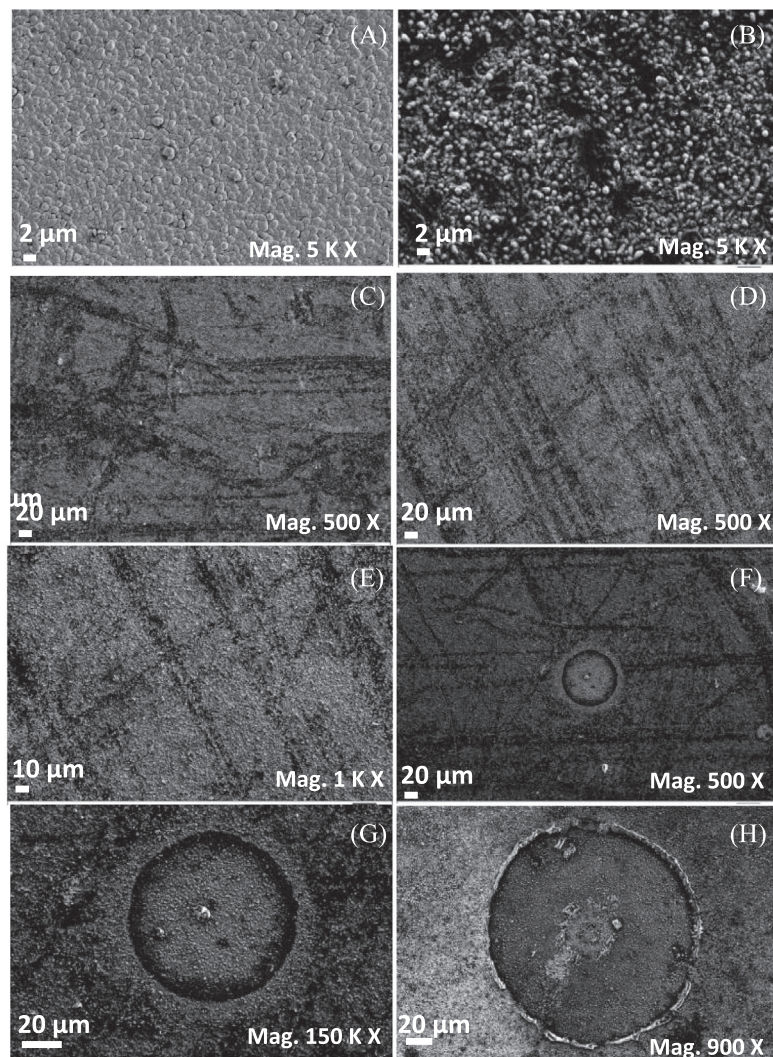
FIGURE 2 FESEM images of top-view of CIGS solar cell at initial and after PID at 1000 V at 85°C for 70 hours (A) initial cell surface microstructure. (B-E), PID treated cell defected surface reveals micro features. (F-H) ring like micro craters formation on surface for PID treated cell (I) Cross-section SEM image of initial and (J) PID treated CIGS solar cell

ring compared to inside crater due extreme compressive strain experienced by the material under PID (see Figure S1 and Table S1). Further, Figure 2I and J shows the cross-sectional view of CIGS solar cell before and after the PID. The granular structure of CIGS layer with no major change has been observed after PID.

3.3 | Compositional study of PID affected cells

The surface compositional analysis of CIGS solar cells for initial sample and after PID treatment has been investigated to probe the evident changes observed from surface
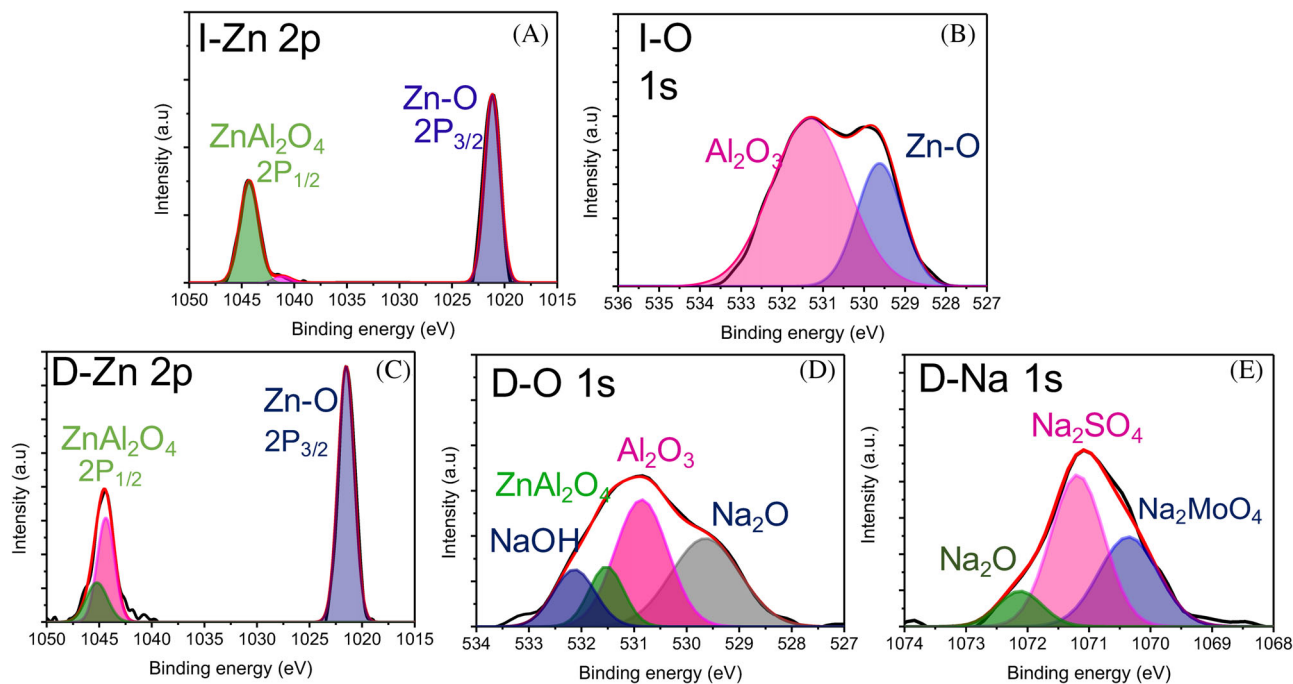
FIGURE 3 Surface chemical analysis of CIGS solar cell for initial and after PID. (A-B), XPS peak of Zn $2p_{1/2}$ and $2p_{3/2}$, O 1s respectively, obtained from initial surface of CIGS solar cell. (C-E), XPS peak of Zn $2p_{1/2}$ and $2p_{3/2}$, O 1s and Na 1s, respectively, obtain

morphology of PID treated cell. The XPS spectra of Zn 2p and O 1s elements were obtained at their respective binding energies at 1044.70 eV, 1021.90 eV and 530.30 eV for initial sample as shown in Figure 3A and B respectively which is in accordance with reported literature.[22] In contrast, XPS spectra for PID treated cells depict an extra at 1072 eV associated to Na 1s elemental peak along with Zn and O peak as denoted by D-O 1s and D-Na 1s in Figure 3D and E, respectively. No significant change has been observed for Zn 2p peak position as compared to initial as shown in Figure 3C. Here, we avoid performing any kind of etching treatment in order to perceive real spectra of the relevant elements after the PID treatment. The changes of the surface chemical composition induced by Na can be further corroborated with change in color of the defected surface where, the Na atoms are more likely to form bonds with O, Mo and S under PID. The presence of Na owed to new chemical compound formation of Na_2O, Na_2SO_4 and Na_2MoO_4 on the surface as shown in Figure 3 F which altered surface composition after PID treatment. In previous reports, Na incorporation has been shown to play a key role towards the progression of PID-s for c-Si.[23,24] A high concentration of Na has appeared due to their drift under the high electric field (2×10^5 V m^{-1}), wherein Na$^+$ ions accelerate from back glass by breaking their dangling bonds with SiO_2. The electric force (eE, where e represents electron charge and E represents the electric field) leads to forward movement of Na$^+$ in the direction of electric field from lower glass substrate towards ZnO layer through CIGS. Availability of O atoms in ZnO leads to formation of Na-O bond and thus annihilation of Na concentration take place, which provides the necessary driving force for the diffusion of Na$^+$ [15]. Concentration of Na$^+$ within ZnO layer builds up with respect to time due to drift and diffusion processes. During this build up Na$^+$ ions puncture the heterojunction of CIGS/CdS layer, which results in a higher leakage current path across the device and leads to a lower shunt resistance.[23] Further, the presence of Na$^+$ reduces the energy split of quasi-Fermi levels by creating excess recombination centers in the heterojunction which manifests lower open-circuit voltage. Comparative higher concentration of Na$^+$ modifies the surface morphology and chemical composition of ZnO as well as CIGS layer towards deterioration of the electrical performance. Extreme defect feature such as surface craters have been critically discussed in next sections.

3.4 | Crystallographic analysis of PID affected cells

The XRD patterns of the initial and PID treated CIGS solar cells are shown in Figure 4. The dominant peaks at 2θ of 28.17°, 36°, 46.0°, 54.25° belong to (112), (211), (204)/(220) and (116)/(312) orientations of polycrystalline chalcopyrite CIGS structure, respectively. In both the cases, initial and after PID show similar characteristic diffraction peaks of CIGS absorber except one extra peak at 37° for PID treated
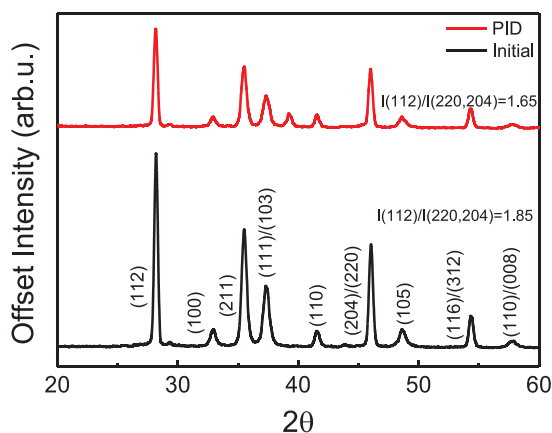
FIGURE 4   XRD patterns of CIGS solar cell for initial before PID and after PID treatment

cell. An extra peak at 37° generated due to PID effect corresponds to the formation of $MoSe_2$ under the presence of Na ions.[25,26] Various reports suggest the formation of $MoSe_2$ layers between CIGS and Mo due to the presence of Na.[26–28] In addition, change in intensities have been observed for PID treated samples. The intensity of the most dominant (112) phase found to be almost half after the PID treatment compared to the initial sample. The maximum peak intensity ratio of I(112)/I(220/204) decreases after PID from 1.85 to 1.65, which indicates the change in crystallinity of CIGS absorber layers under Na migration. The Na induced structural and compositial changes in CIGS absorber layer is consistent with the results reported elsewhere in the literature.[29,30] The different phase and chemical identifications for deteriorated material can be easily detected by Raman analysis as discussed in the subsequent sections, which could not be easily distinguishable by XRD scattering peaks.[31]

3.5 | Raman and optical analysis of PID affected cells

Raman and optical microscopic analysis have been performed to provide an insight towards chemically deformed phases present in the extremely defected regions, especially in the craters. Figure 5 demonstrates Raman spectra of initial and defected cell surfaces. Regions-I, II, III, and IV marked in Figure 5A and B can be clearly distinguished in order to explain deterioration of material under PID. Figure 5C shows the variation in intensity as compared to the initial cell surface. The deviation in intensities indicates structural and compositions alteration induced under PID. The most dominant characteristic peak at 174 cm^{-1} is attributed to A1 mode of lattice vibration for chalcopyrite CIGS layer.[32] The peak intensity of A1 mode increases and shifts from 174 cm^{-1} (for initial surface) to 176 cm^{-1}

for region-I, which signifies microstructural defected surface outside the craters as shown in Figure 5D. The blue shift also signifies that the material experiences compressive strain after PID treatment.[33] Second most dominant peak at 296 cm^{-1} associated with A1 mode refers to the small amount of S remaining in the absorber layer during selenization.[30] Figure 5E also shows a blue shift from 296 to 300 cm^{-1} with significant decrease in intensity which is attributed to compressive strain and crystal disorder induced by Na incorporation. In addition, craters represented by region-II and III reflect dramatically low intensity as compared to main characteristic peak, which is blue shifted from 174 to 177 cm^{-1} as compared to initial as shown in Figure 5D. Further, for II and III regions, second A1 mode shift has been observed from 296 to 302 cm^{-1} as shown in Figure 5G confirms the high order compressive strain inside the material that limits the phonon-phonon vibrations and lowers the scattering intensity of the material.[33] These occurrences can be corroborated to extreme deterioration of CIGS structure. Similarly, region IV reflects blue shift from 296 to 304 cm^{-1} as compared to initial which also indicates the existence of compressive strain for CdS phase at expense of very low intense CIGS A1 phase.

Figure 6 shows PL spectra of initial and PID treated CIGS solar cell. The PL emission intensity found to decrease dramatically after PID. PL spectra can be acquired to understand the recombination of charge carriers and their trapping. The nominal band-gap (E_g) of the CIGS can be estimated in range of 1.20–1.25 eV from the group III elemental composition ratio of 0.4%.[34] PL emission is attributed to mainly recombination of the free charge carriers.[34] The PL emission peaks for initial material has been observed around 1.0–1.2 eV which represents a prominent emission peak. In contrast, the emission intensity reduced significantly for PID treated cell due to an excessive Na migration that induced microstructural defects underlying a complex mechanism after PID, resulting in a loss of radiative recombination. This loss can be due to the altered chemical composition resulting from Na-induced diffusion of Cu, In and Ga elements.[35,36,37] In addition, the extreme deterioration may be owing to a dramatic change in a stoichiometric ratio of Cu/(In+Ga) alteration[35] and a possible deviation in crystal structure. In addition, previous studies have shown that copper vacancies (V_{Cu}^-) are occupied by Na^+ and thus a high concentration of Na_{Cu} point defects exist at the grain boundaries.[27,37,38] The defect pairs of $[Na_{Cu} V_{Cu}]^-$ and $[Na_{Cu} 2V_{Cu}]^{2-}$ have been found stable.[39,40] According to recent report[38,40] the formation of $\{[III_{Cu} V_{Cu}]^+ [Na_{Cu} V_{Cu}]^-\}$ defect super complexes enhances the In/Ga interdiffusion in the CIGS crystal which altered the band-gap profile.
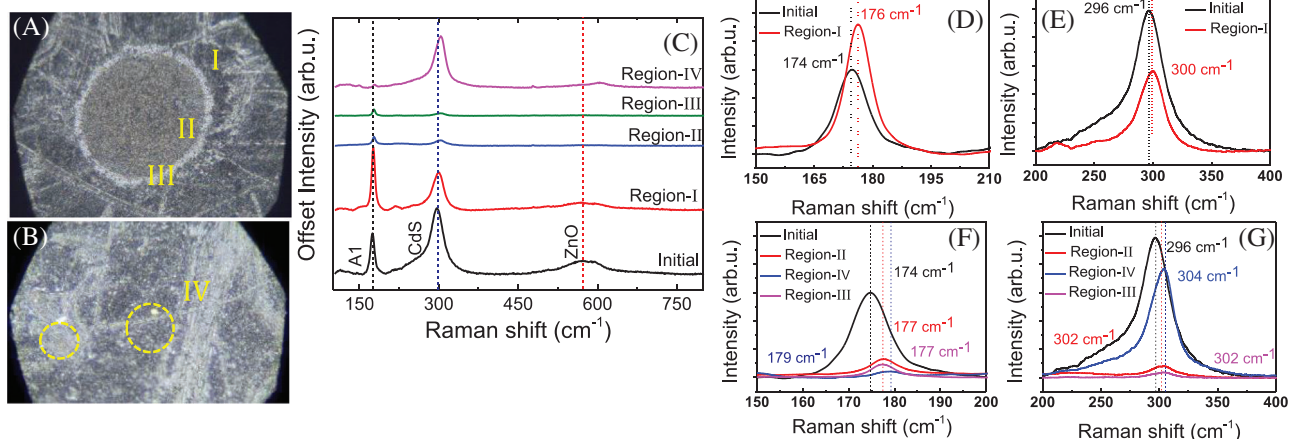
FIGURE 5 Raman shifts of microstructural defected crater (A-B) Raman optical images of PID treated solar cell at -1000 V, 85°C over 70 hours. (C) comparative analysis of different defected regions of craters. D-E, Raman shift of chalcopyrite CIGS after PID and (F-G) Raman shifts of the micro-craters
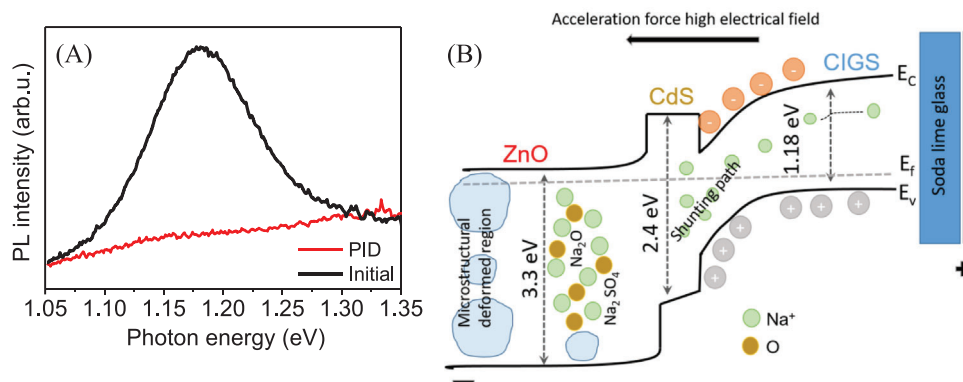

FIGURE 6 (A) Photoluminescence spectra of initial and PID treated cell (B) Schematic representation of degradation mechanism induced by craters under high voltage stress

4 | CONCLUSION

It is evident from recent reports that PID mid-life failure is a challenging issue for PV industries. This needs immediate attention in order to address dramatic reduction in electrical performance degradation of commercial CIGS PV modules. In this article morphological and chemical composition analysis have been reported to investigate fundamental issues behind the onset of material degradation that lead to a drastic reduction in efficiency. The micro-craters on the cell surface observed for the first time after PID have been associated with the crucial modification in elemental and surface composition affecting overall device performance. Na induced defects enhances complex interdiffusion kinetics and the formation of new compounds results in deformation of material to such an extent that changes the energy band profile. The change in band profile promotes recombination and results in significant reduction in open circuit voltage from 0.67 to

0.15 V. This study provides a better understanding of PID failures and their consequences on material properties which can further support the development of effective strategies for PID-free technologies on an industrial scale.

CONFLICT OF INTERESTS

The authors declare that they have no competing interests.

DATA AVAILABILITY STATEMENT

The data that support the findings of this study are available from the corresponding author upon reasonable request.

ORCID

Zeel Purohit https://orcid.org/0000-0001-7785-3245

REFERENCES

1. J. Ramanujam, U. P. Singh, *Energy Environ. Sci.* **2017**, *10*, 1306.
2. P. V. Magazine, Solar Frontier achieves world record thin-film solar cell efficiency of 22.9%. http://www.solar-frontier.com/eng/news/2017/1220_press.html/ (**2017**).
3. B. Beetz, Hanergy's Solibro achieves 18.72% CIGS module efficiency record. PV Mag Int. **2018** https://www.pv-magazine.com/2018/02/02/hanergys-solibro-achieves-18-72-cigs-module-efficiency-record/
4. V. Bermudez, A. Perez-Rodriguez, *Nat. Energy* **2018**, *3*, 466.
5. S. Pingel, O. Frank, M. Winkler, S. Dryan, Potential Induced Degradation of solar cells and panels. 35th IEEE Photovoltaic Specialists Conference, **2010**.
6. W. Luo, Y. S. Khoo, P. Hacke, V. Naumann, D. Lausch, S. P. Harvey, J. P. Singh, J. Chai, Y. Wang, A. G. Aberle, S. Ramakrishna, *Energy Environ. Sci.* **2017**, *10*, 43.
7. P. Hacke Research Opportunities in Reliability of Photovoltaic Modules. National Renewable Energy Laboratory, **2010**.
8. V. Fjallstrom, P. M. P. Salome, A. Hultqvist, M. Edoff, T. Jarmar, B. G. Aitken, K. Zhang, K. Fuller, C. K. Williams, *IEEE J. Photovoltaics* **2013**, *3*, 1090.
9. S. Yamaguchi, S. Jonai, K. Hara, H. Komaki, Y. Shimizu-Kamikawa, H. Shibata, S. Niki, Y. Kawakami, A. Masuda, *Jpn. J. Appl. Phys.* **2015**, *54*, 08KC13.
10. V. Fjallstrom, P. Szaniawski, B. Vermang, P. M. P. Salome, F. Rostvall, U. Zimmermann, M. Edoff, *IEEE J. Photovoltaics* **2015**, *5*, 664.
11. V. Naumann, D. Lausch, A. Hähnel, J. Bauer, O. Breitenstein, A. Graff, M. Werner, S. Swatek, S. Großer, J. Bagdahn, C. Hagendorf, *Sol. Energy Mater. Sol. Cells* **2014**, *120*, 383.
12. D. Lausch, V. Naumann, A. Graff, A. Hähnel, O. Breitenstein, C. Hagendorf, J. Bagdahn *Energy Procedia* **2014**, *55*, 486.
13. M. Theelen, C. Foster, H. Steijvers, N. Barreau, Z. Vroon, M. Zeman, *Sol. Energy Mater. Sol. Cells* **2015**, *141*, 49.
14. M. Theelen, T. Boumans, F. Stegeman, F. Colberts, A. Illiberi, J. Van Berkum, N. Barreau, Z. Vroon, M. Zeman, *Thin Solid Films* **2014**, *550*, 530.
15. D. E. Carlson, R. Romero, F. Willing, D. Meakin, L. Gonzalez, R. Murphy, H. R. Moutinho, M. Al-Jassim, *Prog. Photovolt. Res. Appl.* **2003**, *11*, 377.
16. C. P. Muzzillo, S. Glynn, P. Hacke, H. R. Moutinho, M. R. Young, G. Teeter, I. L. Repins, L. M. Mansfield, *IEEE J. Photovoltaics* **2018**, *8*, 1337.
17. M. Theelen, K. Beyeler, H. Steijvers, N. Barreau, *Sol. Energy Mater. Sol. Cells* **2017**, *166*, 262.
18. D. W. Niles, K. Ramanathan, J. Granata, F. Hasoon, R. Noufi, B. J. Tielsch, J. E. Fulghum, *MRS Proc.* **1997**, *485*, 179.
19. L. E. Oikkonen, M. G. Ganchenkova, A. P. Seitsonen, R. M. Nieminen, *J. Appl. Phys.* **2013**, *114*, 083503.
20. A. Laemmle, R. Wuerz, T. Schwarz, O. Cojocaru-Mirédin, P-Pa Choi, M. Powalla, *J. Appl. Phys.* **2014**, *115*, 154501.
21. D. Shin, J. Kim, T. Gershon, R. Mankad, M. Hopstaken, S. Guha, B. T. Ahn, B. Shin, *Sol. Energy Mater. Sol. Cells* **2016**, *157*, 695.
22. D. W. Niles, K. Ramanathan, F. Hasoon, R. Noufi, B. J. Tielsch, J. E. Fulghum, *J. Vac. Sci. Technol* **1997**, *15*, 3044.
23. J. Bauer, V. Naumann, S. Großer, C. Hagendorf, M. Schütze, O. Breitenstein, *Phys. Status Solidi Rapid Res. Lett.* **2012**, *6*, 331.
24. Z. Purohit, D. Verma, B. Tripathi, *Phys. Chem. Chem. Phys.* **2018**, *20*, 19168.
25. B. B. Wang, K. Ostrikov, T. Van Der Laan, K. Zheng, R. Shao, M. K. Zhu, S. S. Zou, *RSC Adv.* **2016**, *6*, 37236.
26. A. Rockett, K. Granath, S. Asher, M. M. Al Jassim, F. Hasoon, R. Matson, B. Basol, V. Kapur, J. S. Britt, T. Gillespie, C. Marshall, *Sol. Energy Mater. Sol. Cells* **1999**, *59*, 255.
27. P-Pa Choi, O. Cojocaru-Mirédin, R. Wuerz, D. Raabe, *J. Appl. Phys.* **2011**, *110*, 124513.
28. R. Caballero, C. A. Kaufmann, T. Eisenbarth, A. Grimm, I. Lauermann, T. Unold, R. Klenk, H. W. Schock, *Appl. Phys. Lett.* **2010**, *96*, 092104.
29. S. - H. Wei, S. B. Zhang, A. Zunger, *J. Appl. Phys.* **1999**, *85*, 7214.
30. M. Wang, M. Hossain, K. Choy, *Sci. Rep.* **2017**, *7*.
31. A. Nagaoka, Y. Nose, H. Miyake, M. A. Scarpulla, K. Yoshino, *J. Renew. Sust. Energ.* **2015**, *79*, 127.
32. C. M. Ruiz, X. Fontané, A. Fairbrother, V. Izquierdo-Roca, C. Broussillou, S. Bodnar, A. Pérez-Rodríguez, V. Bermúdez, *Appl. Phys. Lett.* **2013**, *102*, 091106.
33. C. Insignares-Cuello, C. Broussillou, V. Bermúdez, E. Saucedo, A. Pérez-Rodríguez, V. Izquierdo-Roca, *Appl. Phys. Lett.* **2014**, *105*, 021905.
34. S. Ishizuka, A. Yamada, M. M. Islam, H. Shibata, P. Fons, T. Sakurai, K. Akimoto, S. Niki, *J. Appl. Phys.* **2009**, *106*, 034908.
35. B. Keyes, F. Hasoon, P. Dippo, A. Balcioglu, F. Abulfotuh, Influence of Na on the electro-optical properties of Cu(In,Ga)Se$_2$. *Conference Record of the 26th IEEE Photovoltaic Specialists Conference*, **1997**.
36. D. Colombara, *Phys. Rev. Mater.* **2019**, *3*, 054602.
37. D. Colombara, K. Conley, M. Malitckaya, H. -. P. Komsa, M. J. Puska, *J. Mater. Chem. A* **2020**, *14*, 6471.
38. L. Kronik, D. Cahen, H. W. Schock, *Adv. Mater.* **1998**, *10*, 31.
39. L. E. Oikkonen, M. G. Ganchenkova, A. P. Seitsonen, R. M. Nieminen, *J. Appl. Phys.* **2013**, *114*, 083503.
40. D. Colombara, F. Werner, T. Schwarz, I. Cañero Infante, Y. Fleming, N. Valle, C. Spindler, E. Vacchieri, G. Rey, M. Guennou, M. Bouttemy, A. G. Manjón, I. Peral Alonso, M. Melchiorre, B. El Adib, B. Gault, D. Raabe, P. J. Dale, S. Siebentritt, *Nat. Commun.* **2018**, *9*, 1.

SUPPORTING INFORMATION

Additional supporting information may be found online in the Supporting Information section at the end of the article.